Journal of Physics: Conference Series

PAPER • OPEN ACCESS

# Instability of wind turbine wakes immersed in the atmospheric boundary layer

To cite this article: Francesco Viola *et al* 2015 *J. Phys.: Conf. Ser.* **625** 012034

View the article online for updates and enhancements.

Related content

- The effect of the number of blades on wind turbine wake - a comparison between 2- and 3-bladed rotors
Franz Mühle, Muyiwa S Adaramola and Lars Sretran
- Identification and quantification of vortical structures in wind turbine wakes for operational wake modeling
Y Marichal, I De Visscher, P Chatelain et al.
- Wind turbine wakes in forest and neutral plane wall boundary layer large-eddy simulations
Josef Schröttle, Zbigniew Piotrowski, Thomas Gerz et al.


IOP ebooks™

Bringing together innovative digital publishing with leading authors from the global scientific community.

Start exploring the collection–download the first chapter of every title for free.

This content was downloaded from IP address 131.114.71.138 on 09/02/2021 at 11:21

Journal of Physics: Conference Series **625** (2015) 012034 doi:10.1088/1742-6596/625/1/012034

# Instability of wind turbine wakes immersed in the atmospheric boundary layer

**Francesco Viola[1], Giacomo Valerio Iungo[2], Simone Camarri[3], Fernando Porté-Agel[4] and François Gallaire[1]**

[1] Ecole Polytechnique Fédérale de Lausanne (EPFL), Laboratory of Fluid Mechanics and Instabilities (LFMI), Lausanne, Switzerland
[2] The University of Texas at Dallas, Mechanical Engineering Department, Wind Fluids and Experiments Lab (WindFluX), 75080 Richardson, TX
[3]Department of Civil and Industrial Engineering, University of Pisa, Pisa 56122, Italy
[4] Ecole Polytechnique Fédérale de Lausanne (EPFL), Wind Engineering and Renewable Energy (WIRE) Lab, Lausanne, Switzerland

E-mail: `Valerio.Iungo@utdallas.edu`

**Abstract.** In this work a technique capable to investigate the near-wake stability properties of a wind turbine immersed in the atmospheric boundary layer is presented. Specifically, a 2D local spatial stability analysis is developed in order to take into account typical flow features of real operating wind turbines, such as the presence of the atmospheric boundary layer and the turbulence heterogeneity of the oncoming wind. This stability analysis can be generally applied on either experimental measurements or numerical data. In this paper it was carried out on wind tunnel experiments, for which a downscaled wind turbine is immersed in a turbulent boundary layer. Through spatial stability analysis, the dominant mode in the near wake, i.e. the most amplified one, is characterized and its frequency matches the hub-vortex instability frequency measured in the wind tunnel. As in the case of [10], where an axisymmetric wake condition was investigated, the hub-vortex instability results in a single-helical mode.

## 1. Introduction

In the wake of wind turbines two main vorticity structures are typically observed: the helicoidal tip vortices and the hub vortex. The tip vortices are shed from the tip of the blades and are rapidly convected downstream because located at the wake periphery where high streamwise velocity is present. The hub vortex is a streamwise-oriented vorticity structure located approximately at the wake centre.

Wind tunnel measurements in the wake produced by a down-scaled wind turbine immersed in a uniform flow showed that these vorticity structures undergo to instabilities in the near-wake and are diffused proceeding downstream [8, 10]. The tip-vortices instability is mainly driven by the mutual inductance between adjacent spirals, in cooperation with short-wave and long-wave instabilities ([1, 2]) which favorite the tip-vortices diffusion within one diameter past the turbine ([3],[4]). Conversely, the hub vortex is characterized by oscillations of a frequency equal to roughly 0.34 times the rotational frequency of the wind turbine rotor which are detected up to two diameters downstream, see [5] and [8]. In previous works these flow fluctuations were ascribed to wake wandering or meandering, which consists in transversal oscillations of the wind


Content from this work may be used under the terms of the Creative Commons Attribution 3.0 licence. Any further distribution of this work must maintain attribution to the author(s) and the title of the work, journal citation and DOI.
Published under licence by IOP Publishing Ltd

turbine wake. Wake meandering was investigated in detail by [5] where it is stated that this phenomenon is mainly excited by the shedding of vorticity structures from the rotor disc acting as a bluff body. In [8], in the case of uniform oncoming flow, this phenomenon was explained as the appearance of a counter-winding and co-rotating single-helix unstable mode amplified in the wake of the wind turbine. More specifically temporal and spatial linear stability analyses were performed on the time-averaged wind tunnel velocity measurements in order to identify the most amplified vortical structures originating at the hub-vortex instability. Furthermore, simultaneous hot-wire measurements confirmed the presence of a helicoidal unstable mode of the hub vortex with a streamwise wavenumber roughly equal to that predicted from the linear stability analysis. This results have been confirmed in the experimental work of [6] where, through laser doppler anemometry (LDA) and particle image velocimetry (PIV) visualization, these authors found that the wake dynamics is associated with a precession (rotation) of the helical vortex core at a constant Strouhal number. Moreover, [7] carried out LES simulations which included all geometrical details of the wind turbine by a curvilinear immersed-boundary method with evidence of large-scale meandering motions.

In [10] a stability analysis is performed by taking into account the effects of the Reynolds stresses by means of eddy-viscosity models. Other studies in the literature have considered eddy-viscosity models to close the linearized equations for the coherent velocity field in a turbulent flow following the seminal work of [9]. In [10] three eddy-viscosity models are considered, where the model parameters are calibrated on the wind tunnel data. One model is based on the assumption of a uniform eddy viscosity for each streamwise location, whereas for the other two models a mixing length is estimated. It was shown that with the proposed improved formulation, stability analysis allows not only the unambiguous identification of the hub vortex instability, but also the accurate frequency prediction.

In the present work the analysis is extended to the case of wind turbines immersed in a turbulent atmospheric boundary layer (ABL). The presence of the ABL in the streamwise direction breaks the axisymmetry of the mean flow, thus the harmonic modal expansion in the azimuthal direction is not valid anymore and a 2D local stability analysis has to be carried out. With this formulation the effect of the condition of the ABL such as shear veer or turbulence heterogeneity on the near wake-dynamics can be included within the present analysis. This formulation is here applied to wind tunnel data acquired in the wake of a downscaled wind turbine subjected to a turbulent oncoming boundary layer flow.
This paper is organized as follows: the wind tunnel data are described in 2, then the formulation of the stability analysis, which takes the modeled Reynolds stresses into account, and the numerical method are presented in 3. The results of the spatial stability analysis of the mean wake flow are then described in 4. Finally, conclusions are drawn in 5.

## 2. Experimental data

In this work a data-set acquired in the boundary layer wind tunnel of the Wind Engineering and Renewable Energy Laboratory (WIRE) of the Ecole Polytechnique Federale de Lausanne (EPFL) has been considered and investigated by 2D local stability analysis. The experimental facility is a closed loop wind tunnel with an inlet providing a contraction with 5:1 area ratio. Several turbulence devices consisting of coarse meshes and honeycomb flow straighteners are used to increase flow quality. The wind turbine down-scaled model used is a three-bladed GWS/EP-6030x3 anticlockwise. The rotor, with a diameter, $d$, of 152 mm, is connected to a DC motor with a diameter of 10 mm. The wind turbine model is mounted with a stem of height 127 mm and is directly installed on the wind tunnel floor. By considering its frontal area, the blockage ratio is less than 0.5%, which is very small to neglect possible effects due to the size of the wind tunnel. More details about a similar experimental setup can be found in [8]. For the tests considered here, the tip speed ratio of the turbine ($TSR$), which is the ratio between

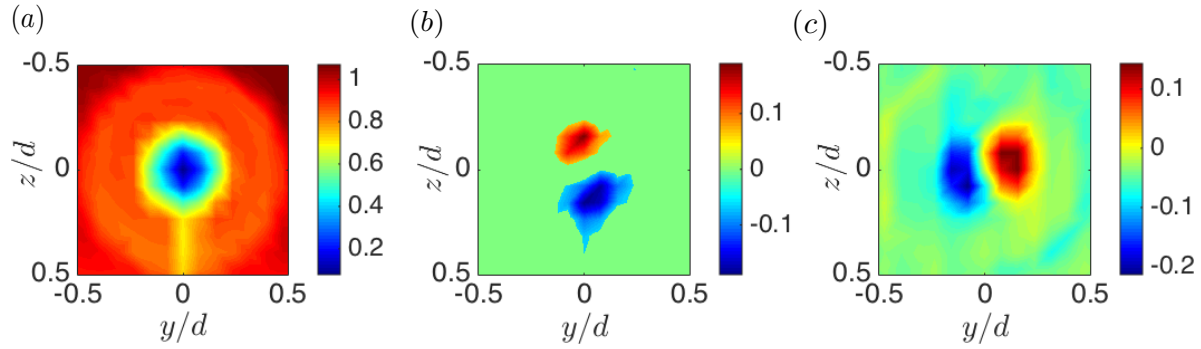


**Figure 1.** Non-dimensional time averaged mean flow at the streamwise position $x/d = 0.375$. (a) $U_x/U_{hub}$, (b) $U_y/U_{hub}$ and (c) $U_z/U_{hub}$.

the speed of the blade tip and the oncoming velocity at hub height, $U_{hub}$, is 4.7. For these tests the mean rotational frequency, $f_{hub}$, was 62 Hz.The velocity at hub height is 6.3 m/s and the turbulence level is equal to 7%. A Reynolds number of 70000 is obtained by considering $U_{hub}$ as reference velocity, and the rotor diameter, $d$, as reference length.

Measurements of three components of the velocity were performed with a customized Cobra probe produced by Turbulent Flow Instrumentation, which is a four-hole pressure probe. This probe, with an external diameter of 1.5 mm, can measure velocity fluctuations characterized by frequencies lower than 300Hz.

The reference frame used has its origin placed just behind the hub of the wind turbine, with the $x$-axis corresponding to the streamwise direction, positive pointing downstream. The $z$-axis is along the vertical direction, positive from the bottom towards the top, while the y-axis is along the spanwise direction oriented so as to produce a right-handed Cartesian coordinate system. Velocity measurements were performed from a downstream distance of $0.375d$ up to $4d$. In figure 1 the three velocity components of the time averaged mean flow field at the streamwise position in the wake $x/d = 0.375$ are shown. In figure 1(a) the streamwise component, $U_x$ is characterized by a strong velocity deficit which is progressively recovered further downstream. The streamwise velocity is higher at the top periphery of the wake than in the lower due to the presence of the ABL and of the sting supporting the turbine. The significant peaks of the spanwise velocity components $U_y$ and $U_z$ (fig. 1(b) and (c) respectively) are detected for radial positions $r/d \approx 0.15$, which are connected to the rotational velocity induced by the hub vortex. In other words the spanwise components correspond to the azimuthal velocity of the hub vortex projected in the cartesian reference frame. The corresponding tangential components of the Reynolds stress tensor are shown in figure 2.

## 3. Stability analysis, turbulent model and numerical method

Following the approach proposed originally by [9] the unsteady flow, $\mathbf{U}(\mathbf{x}, t)$, can be decomposed in three contributions: the time-averaged base-flow, $\overline{\mathbf{U}}(\mathbf{x})$, the coherent fluctuation, $\tilde{\mathbf{u}}(\mathbf{x}, t)$, and the turbulent motion, $\mathbf{u}'(\mathbf{x}, t)$

$$\mathbf{U} = \overline{\mathbf{U}} + \tilde{\mathbf{u}} + \mathbf{u}'$$

Specifically the sum of the time-averaged flow and the coherent fluctuation coincides with the ensemble averaged flow $< \mathbf{U} >= \overline{\mathbf{U}} + \tilde{\mathbf{u}}$. Recalling the formulation detailed in [10] the non-linear evolution of the coherent perturbation, $\tilde{\mathbf{u}}$, on top of the time averaged mean flow, $\overline{\mathbf{U}}$, is given

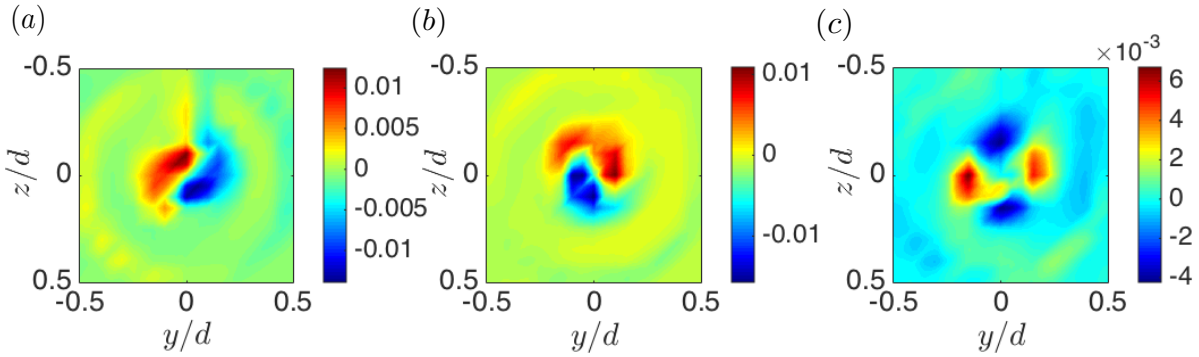


**Figure 2.** Non-dimensional tangential components of Reynolds stress tensor at the streamwise position $x/d = 0.375$. (a) $\overline{u'_x u'_y}/U^2_{hub}$, (b) $\overline{u'_x u'_z}/U^2_{hub}$ and (c) $\overline{u'_y u'_z}/U^2_{hub}$.

by the equation (1):

$$\begin{gathered}\nabla \cdot \tilde{\mathbf{u}} = 0 \\ \frac{\partial \tilde{\mathbf{u}}}{\partial t} + \nabla\tilde{\mathbf{u}} \cdot \overline{\mathbf{U}} + \nabla\overline{\mathbf{U}} \cdot \tilde{\mathbf{u}} = -\nabla\tilde{p} + \frac{1}{\mathrm{Re}}\Delta\tilde{\mathbf{u}} - \nabla \cdot [\tilde{\mathbf{u}}\tilde{\mathbf{u}} - \overline{\tilde{\mathbf{u}}\tilde{\mathbf{u}}}] - \nabla \cdot [< \mathbf{u}'\mathbf{u}' > - \overline{\mathbf{u}'\mathbf{u}'}]\end{gathered} \tag{1}$$

where the third and last terms of the rhs are respectively the non-linear term and the difference among the Reynolds stresses obtained by ensamble and time averages. From now on, the equations are made non-dimensional with the turbine diameter $d$ and the velocity at the hub $U_{hub}$. In the linear framework the coherent perturbation is assumed to be small and by using the Boussinesq approximation for the Reynolds stresses, eq. (1) is rewritten as follows:

$$\frac{\partial \tilde{\mathbf{u}}}{\partial t} + \nabla\tilde{\mathbf{u}} \cdot \overline{\mathbf{U}} + \nabla\overline{\mathbf{U}} \cdot \tilde{\mathbf{u}} = -\nabla\tilde{p} + \frac{1}{\mathrm{Re}}\Delta\tilde{\mathbf{u}} + \nabla \cdot (\nu_t(\overline{\mathbf{U}})[\nabla + \nabla^T]\tilde{\mathbf{u}}) + \nabla \cdot ((\nabla_{\mathbf{U}}\nu_t(\overline{\mathbf{U}}) \cdot \tilde{\mathbf{u}})[\nabla + \nabla^T]\overline{\mathbf{U}}) \tag{2}$$

Equation(2) is the linear evolution of the coherent perturbation on a turbulent time-averaged mean flow with enforced Boussinesq hypothesis, where the eddy-viscosity terms need to be modeled. As in [10] we adopt here the generalized mixing-length model, hence $\nu_t$ is given by:

$$\nu_t = l_m^2 (2\overline{S} : \overline{S})^{1/2} \tag{3}$$

where $S$ is the strain rate tensor. The mixing-length $l_m$ is tuned on the experimental data through a best fit procedure on the Boussinesq equation, in a similar way to [10]. This is done separately at each streamwise section considered for the local stability analysis, so that the value of $l_m$ varies with $x$. The term $\nabla_{\mathbf{U}}\nu_t \cdot \tilde{\mathbf{u}}$ represents the eddy-viscosity variation due to the coherent fluctuation and it is given by the linearization of the model around the mean flow:

$$\nabla_{\mathbf{U}}\nu_t(\overline{\mathbf{U}}) \cdot \tilde{\mathbf{u}} = l_m^2 \frac{2\overline{S} : \tilde{s}}{(2\overline{S} : \overline{S})^{1/2}} \tag{4}$$

In the framework of weakly-non-parallel stability analysis, eq. (2) is now applied to a parallel flow $\overline{\mathbf{U}} = (\overline{U}_x(y,z), \overline{U}_y(y,z), \overline{U}_z(y,z))$ extracted at a given streamwise location. Note that, the three components of the time averaged mean flow vary in both spanwise directions $y$ and $z$, consequently the local analysis is bidimensional. In contrast, the $x$-dependence of the flow is considered by carrying out different stability analysis at different sections in the wake, as typical

in local analysis assuming weak variations of the flow in that direction. This allows for a modal expansion of the coherent fluctuation in the following form:

$$\tilde{\mathbf{u}}(x,y,z,t) = \hat{\mathbf{u}}(y,z)\exp(i(kx-\omega t)) \tag{5}$$

where $k$ is axial wavenumber and $\omega$ is the frequency. When this modal form is substituted in Eq. (2), an eigenvalue problem is obtained and eigenfunction solutions exist only if $k$ and $\omega$ satisfy a dispersion relation of the form:

$$D[k,\omega] = 0. \tag{6}$$

The spatial branches, which describe the amplification of perturbation in space, are obtained by solving the dispersion relation with complex wavenumbers $k$, and real frequency $\omega$, have been considered here (see [8]). Given $k = k_r + ik_i$, $i$ being the imaginary unit, the term $-k_i$ is the spatial amplification rate, while $k_r$ corresponds to the streamwise wavenumber of the traveling pertubation with frequency $\omega$. Due to the weakly non-parallelism of the meanflow, $\overline{\mathbf{U}}$, the derivatives in the streamwise direction are of higher order and the term $2\overline{S} : \overline{S}$ appearing in equation (3) at leading order reduces to:

$$(2\overline{S} : \overline{S})^{1/2} \approx \left[\left(\frac{\partial \overline{U}_x}{\partial y}\right)^2 + \left(\frac{\partial \overline{U}_x}{\partial z}\right)^2 + \left(\frac{\partial \overline{U}_y}{\partial z} + \frac{\partial \overline{U}_z}{\partial y}\right)^2 + 2\left(\frac{\partial \overline{U}_y}{\partial y}\right)^2 + 2\left(\frac{\partial \overline{U}_z}{\partial z}\right)^2\right]^{1/2} \tag{7}$$

Similarly the term $2\overline{S} : \tilde{s}$ in the expression of the eddy-viscosity variation due to the coherent fluctuation (4) is given by:

$$\begin{aligned} 2\overline{S} : \tilde{s} \approx{}& \left(\frac{\partial \overline{U}_x}{\partial y}\right)\left(\frac{\partial \tilde{u}_x}{\partial y} + \frac{\partial \tilde{u}_y}{\partial x}\right) + \left(\frac{\partial \overline{U}_x}{\partial z}\right)\left(\frac{\partial \tilde{u}_x}{\partial z} + \frac{\partial \tilde{u}_z}{\partial x}\right) + \left(\frac{\partial \overline{U}_y}{\partial z} + \frac{\partial \overline{U}_z}{\partial y}\right)\left(\frac{\partial \tilde{u}_y}{\partial z} + \frac{\partial \tilde{u}_z}{\partial y}\right) \\ &+ 2\left(\frac{\partial \overline{U}_y}{\partial y}\right)\left(\frac{\partial \tilde{u}_y}{\partial y}\right) + 2\left(\frac{\partial \overline{U}_z}{\partial z}\right)\left(\frac{\partial \tilde{u}_z}{\partial z}\right) \end{aligned} \tag{8}$$

Equations (2) together with modal expansion (5) are discretized using a staggered pseudospectral Chebyshev-Chebyshev collocation method. The three velocity components are defined at the Gauss-Lobatto-Chebyshev (GLC) nodes, whereas the pressure is staggered on a different grid, which is generated with Gauss-Chebyshev nodes (GC). In both $y$ and $z$ directions the algebraic mapping with domain truncation is used, in order to cluster the nodes at the wake center. In the present work $N_y = 40$ and $N_z = 40$ points are used in the axial and radial direction respectively, this resolution having shown to provide the desired convergence of the amplification factors.

## 4. Hub vortex instability

The local spatial analysis has been carried out at several streamwise positions in the wake of the wind turbine where the experimental data were acquired. In figure 3 the results of the spatial analysis at the first available section, $x/d = 0.375$, are reported. In fig. 3(a) the spatial growth rates $-k_i$ are depicted as a function of the frequency of the coherent fluctuation $\omega$, while in (b) the associated axial wavenumbers are shown. Three modes, labeled as modes 1, 2 and 3, result to be amplified in the frequency band $0 \leq \omega \leq 7$. In particular, in the frequency range $2.5 \leq \omega \leq 4$ the three modes coexist and three unstable eigenvalues are found when carrying out the stability analysis. Each mode is characterized by a *preferred* frequency, defined

as the frequency associated with the higher spatial growth-rate, which is equal approximately to 2.7 for mode 1, to 5 for mode 2 and to 2.8 for mode 3. In figure 4 the axial velocity of the eigenmodes 1, 2 and 3 at the respective preferred frequency, are reported, showing that: the detected unstable modes and related branches present different spatial structures. Specifically, in fig. 4(a-d) the complex eigenfunction clearly exhibit a dominant single-helical shape, which is in agreement with the stability analysis results in the wake of a wind turbine invested by a uniform oncoming flow ([8, 10]) even though in this analysis no modal expansion is imposed in the azimuthal direction and eigenfunctions can have a generic shape in the $y-z$ plane. The eigenfunction of mode 2 in fig. 4(b-e) represents a double-helical mode. Lastly, the mode 3 in (c-f) is dominated by a single-helical symmetry, but more diffused respect to mode 1.

By observing the spatial growth rates in fig. 3(a), the most amplified perturbation at $x/d = 0.375$ is the single-helical mode 1 at the dominant frequency $\omega = 2.7$. The same analysis has been carried out in the other streamwise sections in the wind turbine wake and a similar scenario is obtained, with the single helix mode 1 more amplified at the low frequency range. However proceeding downstream the spatial growth rates reduce due to the recovery of the wake deficit and the increase of the turbulence intensity which favorites the diffusion of the vortex structures.

In order to determine the most amplified coherent fluctuation through the wake and its frequency, the local spatial growth rates are integrated in the streamwise direction according to:

$$G(\omega) = \exp \int_{x_i}^{x_s} -k_i(\omega, x)\mathrm{d}x. \tag{9}$$

The global gain represents the integral measure of the amplification in the wake between the first section available, $x_i = 0.375d$, and $x_s$ which is the streamwise position where the mode becomes stable. $G(\omega)$ is reported in figure 5 as a function of the frequency $\omega$, where the three modes amplified in the wake are labeled as before. Therefore mode 1 results to be the most amplified mode overall and its dominant frequency is in good agreement with the hub-vortex instability frequency measured in the wind tunnel, whose non-dimensional value is $\omega \approx 3$ and is depicted by the red line in fig. 5. The limited deviation in the frequency prediction is believed to be related to a non-linear modulation which can not be captured by this linear stability approach.
The velocity field of the coherent perturbation at a given frequency $\omega$ is given by equation (10)

$$\tilde{\mathbf{u}}(x, y, z, t) = Re\left\{\hat{\mathbf{u}}(x; y, z)e^{i(\int_{x_i}^{x} k(x',\omega)\mathrm{d}x' - \omega t)}\right\}. \tag{10}$$

Hence, at a given time the term $e^{i\int_{x_i}^{x} k_r(x')\mathrm{d}x'}$, where $k_r(x)$ is the local wavenumber, is setting the phase of the local complex eigenfunction $\hat{\mathbf{u}}(x; y, z)$. Since the $k_r(x)$ are positive quantities, the phase increases proceeding downstream, providing different orientations to the local velocity field yielding the typical helical shape of the hub-vortex instability, see [8]. Consequently, the unsteady term $e^{-i\omega t}$ consists in a uniform change of phase in time, resulting in a constant rate rotation of the perturbation around its axis. The axial velocity of mode 1 at frequency $\omega = 2.7$, which is the most amplified coherent perturbation according to spatial analysis, is reported in figure 6 at different streamwise positions in the wind turbine wake. In all the considered sections the single-helical symmetry is the dominant one. Moreover, by moving downstream, the eigenfunction is less concentrated around the hub-vortex core due to turbulent diffusion, as known by experimental evidence. Hence, also in this case of wind turbine immersed in the atmospheric boundary layer the hub-vortex instability is associated with an helical precession of the vortex-core. Moreover, it is interesting to notice that while proceeding downstream, the helicoidal structure observed is slightly displaced downwards. This feature can be related to the presence of the boundary layer. This general lowering of the wake vorticity structures is also typically observed for wakes produced by bluff bodies immersed in a boundary layer, as for the case for a triangular prism in [11].

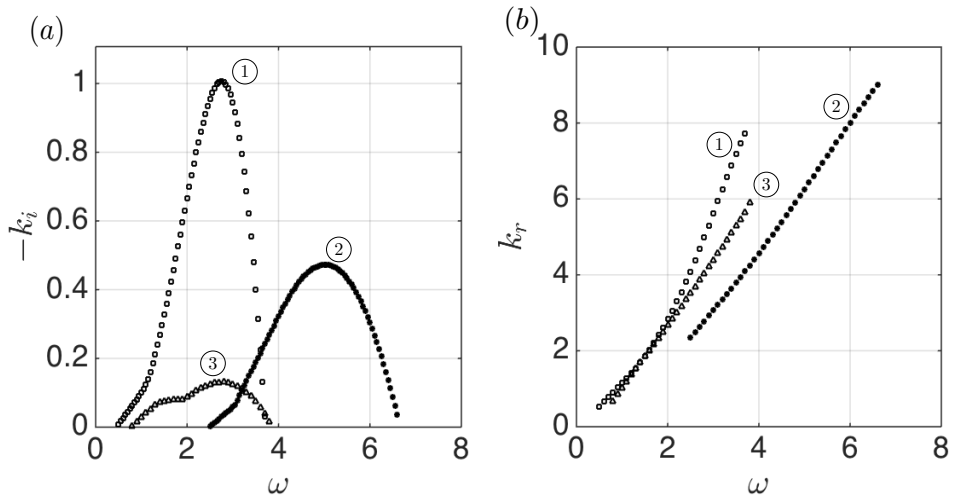


**Figure 3.** Spatial analysis results at the section $x/d = 0.375$. In (a) the growth rates, $-k_i$, are reported as a function of the frequency $\omega$, while in (b) the corresponding axial wavenumbers, $k_r$, are shown. Each branch corresponds to a different amplified mode.

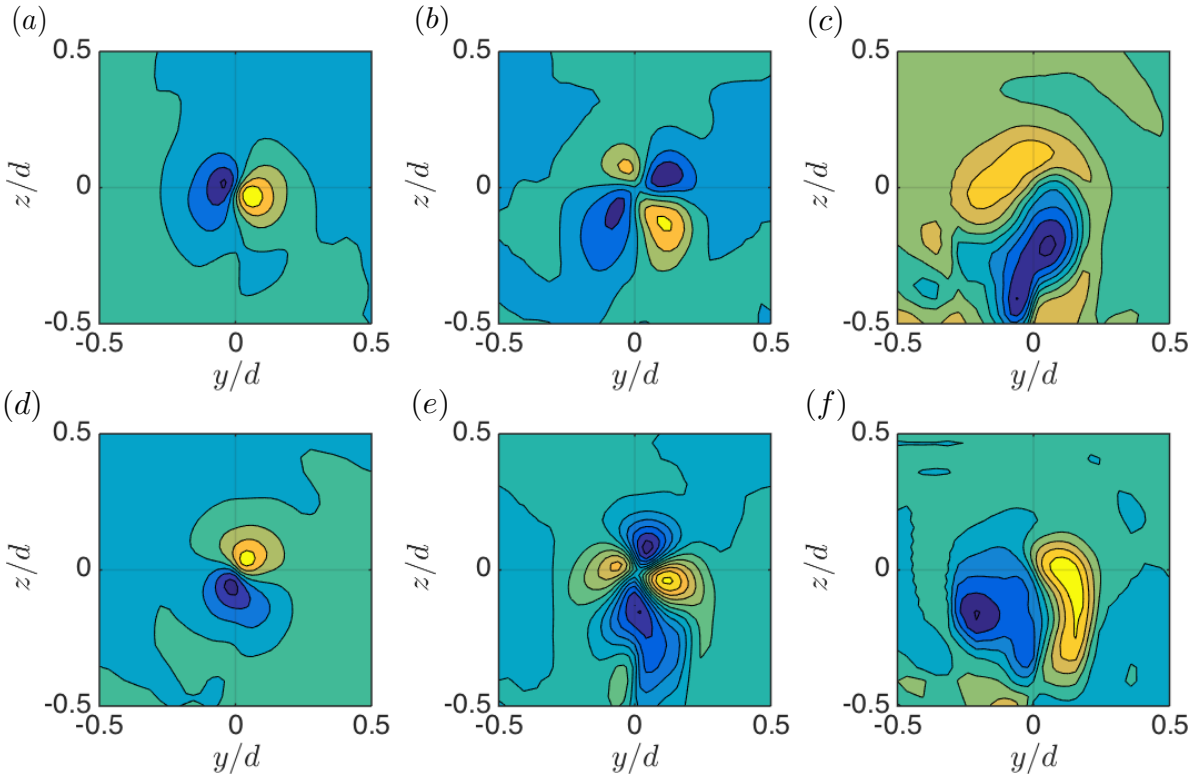


**Figure 4.** Spatial analysis results at the section $x/d = 0.375$. Real (a) and imaginary (d) part of the axial flow of the eigenfunction associated to mode 1 at frequency $\omega = 2.7$. In (b) and (e) the same quantities are shown for mode 2 at frequency $\omega = 5$ and in (c) and (f) for mode 3 at frequency $\omega = 2.8$.

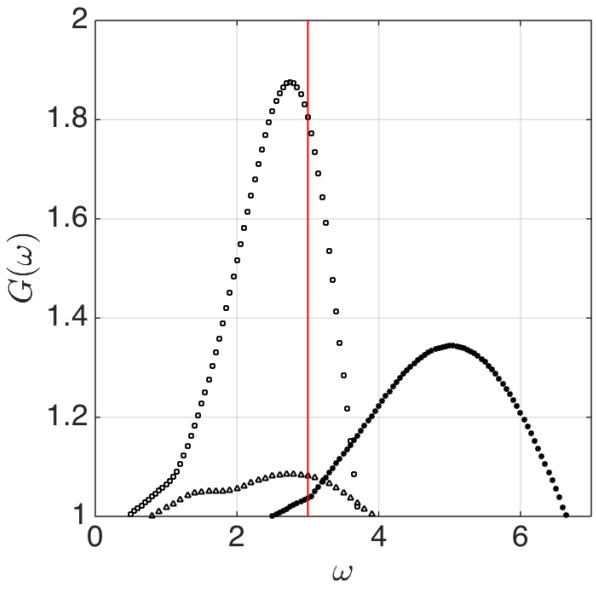


**Figure 5.** Integral amplification factor of coherent perturbations in the wake as a function of the frequency $\omega$. Three modes, labeled as mode 1, mode 2 and mode 3 are amplified through the domain.The vertical red line represents the frequency of the hub vortex instability measured experimentally, corresponding to a non-dimensional pulsation $\omega_{hubvortex} = 3$.

## 5. Conclusions

A method suitable for local stability analysis in the near wake of wind turbine wakes has been developed and here presented. The method is based on the triple decomposition of the flow field, where an equation describing the dynamics of the coherent perturbations on the time-averaged flow and taking into account the turbulent diffusion is provided. Due to the weakly non parallelism of the flow in the case of wind turbine wakes, a local stability approach has been adopted. More specifically, at a given streamwise position in the wake, $x$, both $y$ and $z$ directions are discretized by using Chebyshev polynomials and the spatial amplification of perturbations as a function of the frequency are computed. Thus, in this method no modal expansion is imposed to the geometry of the perturbation in the azimuthal direction and the modes investigated are allowed to have a generic shape in the $y-z$ plane. Conversely, a complex wavenumber $k$ is given, where its real and imaginary part define respectively the axial wavelength of the perturbation and its spatial amplification.

In this framework the effect on the near-wake dynamics of typical flow features of the incoming wind, such as the atmospheric boundary layer, turbulence heterogeneity, veer and shear, can be included in the stability analysis. Hence, real operating wind turbines conditions can be investigated with the present tool.

The analysis has been here applied on wind tunnel data, where the mean wind direction is aligned with the wind turbine axis. In particular, the mean wake flow acquired in the wind tunnel is used directly in the stability analysis and the measured Reynolds stresses are used to tune the mixing-length model, which is adopted to take into account turbulent diffusion in the dynamics of the hub-vortex instability. The local spatial growth rates are computed at every streamwise position in the wake as a function of the frequency of the perturbation. Three modes, which manifest a dominant helical shape, are found to be amplified in the wake. Specifically, the single helical mode 1 is more unstable in the low frequency range $0 \leq \omega \leq 4$, conversely the double helical mode 2 resonates in the higher frequency interval $4 \leq \omega \leq 6.5$. Finally mode 3 results to be less amplified than modes 1 and 2 in all the frequency range. The dominant mode

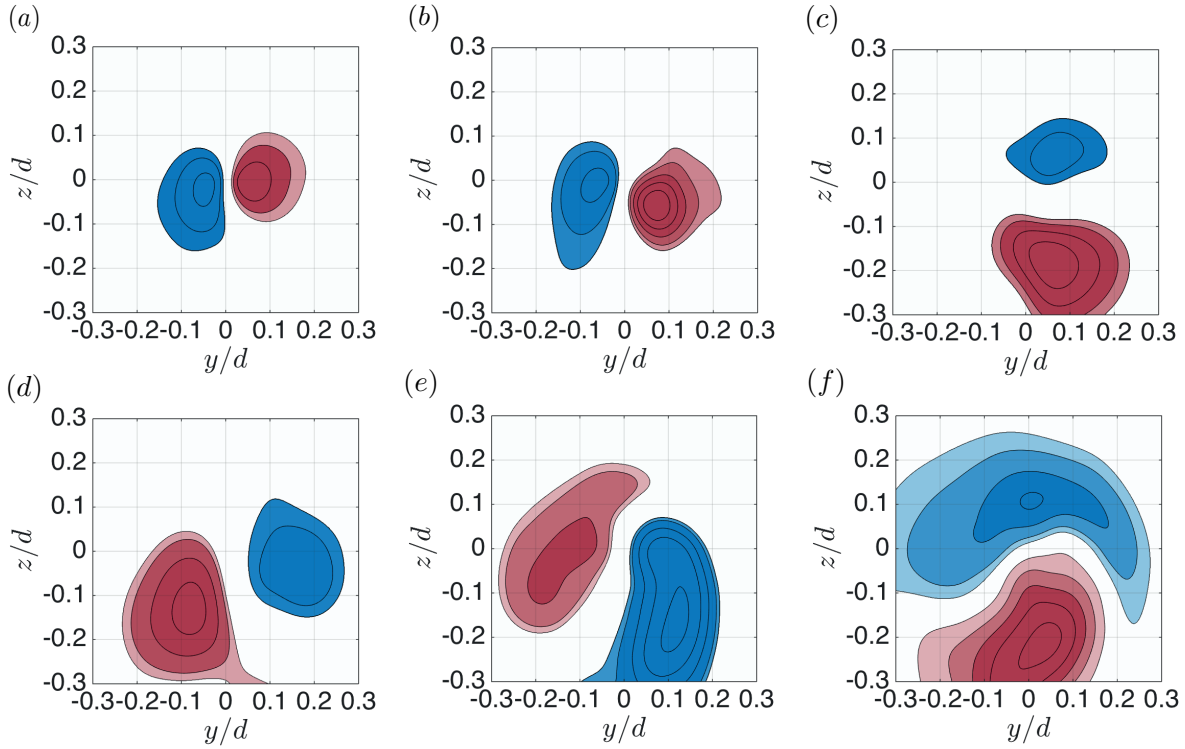


**Figure 6.** Axial velocity of the most amplified coherent perturbation (mode 1 with frequency $\omega = 2.7$) at different streamwise positions. (a) $x/d = 0.375$, (b) $x/d = 0.50$, (c) $x/d = 0.75$, (d) $x/d = 1.00$, (e) $x/d = 1.50$ and (f) $x/d = 2.00$.

in the wind turbine wake, and its frequency, are detected by means of the integral amplification factor, which is obtained by integrating the spatial growth rates for the different downstream locations. The spatial shape of this resonating vorticity structure results mode 1, i.e. a single-helix in agreement with previous works which is a remarkable result recalling that no azimuthal modal expansion has been applied to the perturbation field. Moreover, the frequency predicted for the most unstable mode is in good agreement with the one measured in the wind tunnel.

The applicability of this 2D spatial local stability analysis is very general since it is suitable to be directly used to investigate the wake stability of wind turbine flows experimentally measured in the wind tunnel, wind LiDARs, or simulated by RANS or LES approaches.

## References

[1] Widnall S E, 1972, J. Fluid Mech. 54 (4), 641-663
[2] Felli M, Camussi R and DiFelice F, 2011, J. Fluid Mech. 682, 5-53.
[3] Sarmast S, Dadfar R, Mikkelsen R F, Schlatter P, Ivanell S, Sørensen J N and Henningson D S, 2014, J. Fluid Mech. 755, 705-731.
[4] Zhang W, Markfort C D and Porté-Agel F, 2012, Exp. in Fluids. 52-5, 1219-1235.
[5] Medici D, and Alfredsson P H, 2008 Wind Energy 11, 211-217.
[6] Okulov V L, Naumov I V, Mikkelsen R F, Kabardin I K and Sørensen J, 2014, J. Fluid Mech. 747, 369-380.
[7] Kang S, Yang X and Sotiropoulos F, 2014, J. Fluid Mech. 744, 376-403.
[8] Iungo G V, Viola F, Camarri S, Porté-Agel F and Gallaire F 2013 J. Fluid Mech. 737 499-526
[9] Reynolds W C and Hussain K M, 1972 J. Fluid Mech. 54, 263-288.
[10] Viola F, Iungo G V, Camarri S, Porté-Agel F and Gallaire F 2014 J. Fluid Mech. 750 R1
[11] Buresti G and Iungo G V 2010 J. Wind Eng. Ind. Aerodyn. 98 253262